Enhancement of Radiative Plasmon Decay by Hot Electron Tunneling

Xiao Wang,* Kai Braun, Dai Zhang, Heiko Peisert, Hilmar Adler, Thomas Chassé, and Alfred J. Meixner*

Institute of Physical and Theoretical Chemistry and LISA+, University of Tübingen, Auf der Morgenstelle 18, 72076 Tübingen, Germany

ABSTRACT

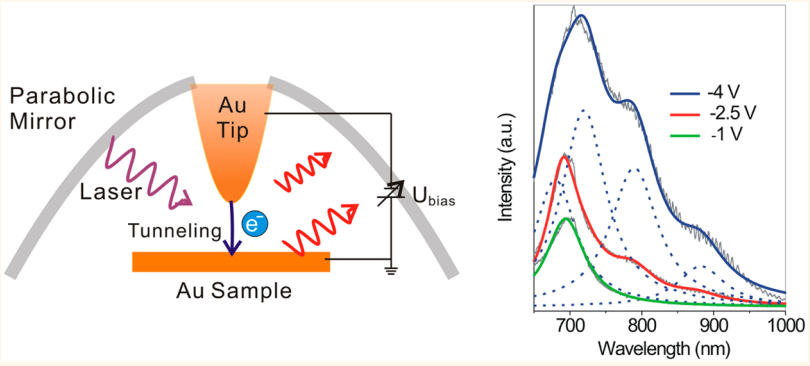

Here we demonstrate that photon emission induced by inelastic tunneling through a nanometer single gap between a sharp Au tip and an Au substrate can be significantly enhanced by the illumination of the junction with 634 nm laser light with an electric field component oriented parallel to the tip-axis, *i.e.*, perpendicular to the sample. Analyzing photoluminescence (PL) spectra recorded as a function of bias voltage allows us to distinguish between PL from (1) the decay of electron−hole pairs created by the laser excited sp/d interband transition with a characteristic band at 690 nm and (2) the red-shifted radiative decay of characteristic plasmon modes formed by the gap. Since the electroluminescence spectra (without laser) already show the plasmonic gap modes, we conclude that the enhanced intensity induced by laser illumination originates from the radiative decay of hot electrons closely above the Fermi level *via* inelastic tunneling and photon emission into the plasmon modes. Since these processes can be independently controlled by laser illumination and the amplitude of the bias voltage, it is of great interest for designing new switchable photon emission plasmonic devices.

KEYWORDS: tip-enhanced near-field optical microscopy · hot electrons · plasmons · inelastic electron tunneling

Owing to the optical excitation of localized surface plasmons (LSP), noble metal nanostructures have the ability to concentrate light from free space into nanometer scale volumes, providing strongly enhanced optical fields near the nanostructures.[1,2] For two closely spaced metallic nanostructures interacting with incident light, their surface plasmons are coupled by the optical near-field confined in the gap.[3] By varying the size of the nanometer gap, plasmonic coupling and the enhanced optical fields can be controlled,[4−7] which is highly desirable for various applications, such as high sensitive chemical and biological sensing.[8,9] On the basis of the same principle, in the so-called tip-enhanced near-field optical microscopy,[10] excited with laser light polarized along the tip axis, strong optical near-fields are created and confined in the tip−sample gap, which greatly enhance the optical processes such as Raman scattering and photoluminescence (PL).[11,12] Due to the large optical enhancements in nanoscale volumes, tip-enhanced near-field optical microscopy can reach an optical resolution dramatically below the diffraction limit[13−19] and a sensitivity at the single molecule level.[20,21] LSP can also be excited by electrons. One approach is by inelastic electron tunneling (IET) across a nanogap formed by a metal tip and a substrate in a scanning tunneling microscopy (STM) with optical access.[22−24] The size of the nanogap can be controlled precisely by the STM feedback mechanism. Electrically excited plasmon resonances confined by the STM junction can be tuned by varying the tip or the sample status.[25,26] Because of the high spatial confinement of the electron tunneling, optical resolutions

* Address correspondence to xiao.wang@uni-tuebingen.de; alfred.meixner@uni-tuebingen.de.

Received for review April 20, 2015 and accepted July 22, 2015.

Published online July 22, 2015
10.1021/acsnano.5b02361

down to submolecular level from various samples can be achieved.[27,28]

Recently, the interest in studying quantum effects in a coupled plasmonic systems at small separations has increased dramatically. When the gap narrows from nanometers to atomic length scales, recent publications show that the plasmonic system enters the quantum regime in which coherent quantum tunneling of electrons establishes a limit for plasmonic confinement.[29,30] However, the mechanism is still a controversial issue, since effects of the nonlocality of the metal dielectric function at tunneling distances could provide for similar experimental observations.[7] Furthermore, how the optically excited plasmons interact with the electrically excited plamons in the same nanogap still remains unclear. The combination of laser illumination and bias voltage variation in a tunneling junction provides a chance to study the interplay of plasmon excited hot electrons and conduction electrons inelastic tunneling.

Since the weak PL of gold that originates from radiative recombination of sp-band electrons and d-band holes is enhanced by surface plasmons resonance, the spectral line shape of the PL is also influenced by the plasmon resonance of the system.[7,31,32] In this paper, we study bias voltage dependent laser-induced PL spectra of an Au−Au junction in a home-built tip enhanced near-field optical microscope with tunneling current as the tip−sample distance feedback signal. We investigate the IET excited LSP by collecting electroluminescence spectra from the same junction without laser illumination. Finally, we demonstrate electron tunneling mediated amplification of PL of the Au−Au junction.

RESULTS AND DISCUSSION

A sketch of the experimental configuration is shown in Figure 1a. The Au tip working as an optical antenna is made by electrochemical etching of an Au wire (diameter of 100 μm) in HCl solution. Figure 1b shows the scanning electron micrograph of the tip used in this study. The sample consists of an Au(111) crystal, which is cleaned in piranha solution[20] before the experiments. A radially polarized diode laser beam (634 nm, 170 μW) is used as the optical excitation source. A parabolic mirror serves as the focusing element.[33] The Au−Au junction is formed by first positioning the Au tip into the focus of the parabolic mirror and then approaching the Au crystal toward the tip until a tunneling current is observed. As the laser beam is radially polarized, the electric field in the focus oscillates mainly parallel to the tip axis,[34,35] which

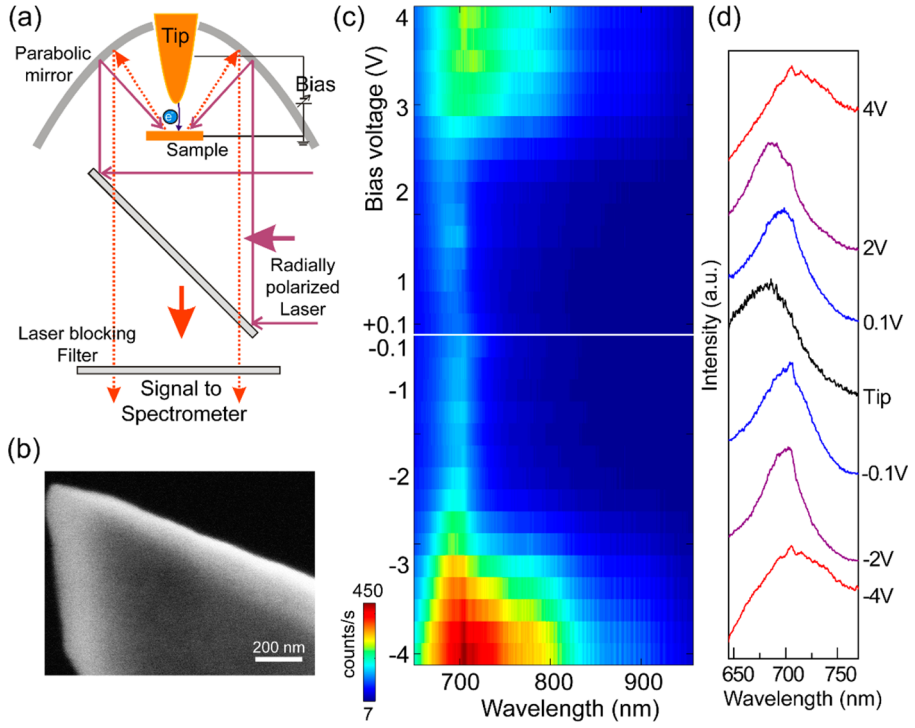

Figure 1. (a) Sketch of the experimental configuration. A radially polarized laser beam at 634 nm is focused by a parabolic mirror with a numerical aperture of NA ≈ 1 on the Au-tip Au-sample junction. The luminescence from the junction is collected by the same mirror and directed *via* a laser line blocking filter to a spectrograph equipped with a liquid N_2 cooled CCD-detector for recording spectra. A bias voltage is applied between the tip and the sample to induce electron tunneling. (b) Scanning electron micrograph image of the gold tip used in the experiments. (c) 2-D plot of the PL spectra recorded with constant laser intensity (170 μW) as a function of bias voltage (U_{bias}) varying from −4 to 4 V. U_{bias} varies in steps of ±0.25 V in the range from ±1 to ±4 V. For U_{bias} smaller than ±1 V, only emission spectra at ±0.1 and ±0.5 V were collected. (d) Enlarged PL spectra in the spectral range from 645 to 770 nm at typical bias voltages and the PL spectrum of the Au tip only. The spectra are normalized and offset for clarity.

would excite the junction more efficiently as compared to the linear polarization. Under these conditions, electrons are efficiently excited from the d-band to the sp-band above the Fermi-level leaving holes in the d-band. For the same Au−Au junction, electroluminescence (EL) spectra can be recorded as a function of bias voltage purely by IET. In combination with laser excitation under the identical conditions, we observe a 2 orders of magnitude intensity increase of the Stokes shifted optical signal. Negative and positive bias voltages all refer to the polarity of the tip. The experiments were performed with a constant tunneling current of 1 nA in ambient conditions and at room temperature. The tip−sample distance is estimated to be about 1 nm and an increase by 0.16 nm when bias voltage is raised from |±0.1| V to |±4| V. This tiny increase of the distance would only slightly decrease the near-field coupling strength between the tip and the sample, resulting in less enhanced optical signal from the junction. Since we observe an increase of the optical signal at higher bias voltages, tip−sample distance increase cannot be the cause for the observed phenomena. Furthermore, the general light emission behavior is reproducible with other tips and surfaces.

Figure 1c shows 2-D plot of stacked PL spectra of the Au−Au junction as a function of bias voltage varying from −4 to 4 V. The intensity of the spectra is indicated by the color. Along with the PL spectrum of the Au tip only, the enlarged PL spectra in the range from 645 to 770 nm recorded at typical bias voltages are shown in Figure 1d. Over the whole range of bias voltage, we observe dramatic changes in both the spectral profile and the PL intensity. From Figure 1c it is clearly visible that, at low bias voltages ($|U_{bias}| < 1.75$ V), the PL spectrum has only one clear emission maximum and the spectrally integrated intensity is almost independent of the bias voltage. Compared to the PL spectrum observed from the bare gold tip (black curve in Figure 1d), the PL spectra of the laser illuminated junction recorded at bias voltages of ±0.1 V (blue curves in Figure 1d) are red-shifted by about 10 nm. The spectral red-shift is caused by the plasmonic tip−sample coupling at a small gap.[36] For higher bias voltages ($|U_{bias}| \geq 1.75$ V), a significant increase of PL intensity is observed and spectral shoulders at about 780 and 880 nm arise in Figure 1c. Despite higher intensities observed at larger negative bias voltages, in general, the PL spectra vary in a similar manner for positive and negative bias voltages. Changes in the PL spectral line shape indicate that LSP modes generated by IET at higher bias voltages contribute to the spectra. To elucidate how IET is involved in the mechanism of the enhanced PL emission at higher bias voltage, we will analyze the LSP modes generated by pure IET in the very same junction in the next section of this article.

EL from Au−Au junctions has been well studied under ultrahigh vacuum (UHV) conditions at room[23,37,38]

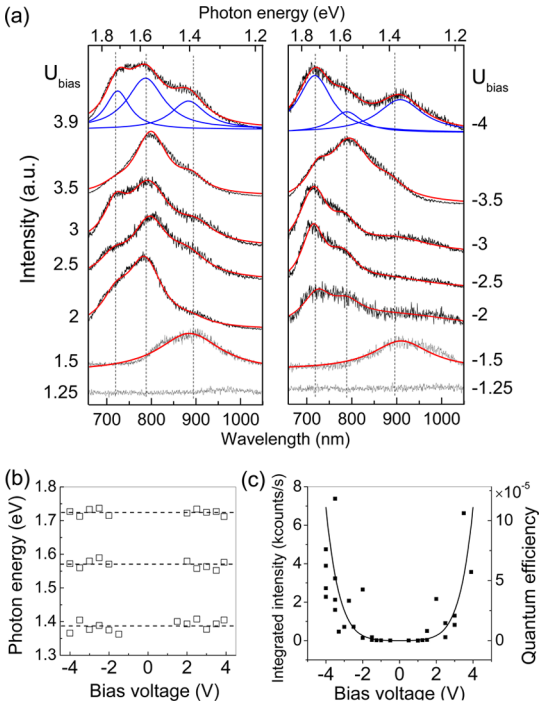

Figure 2. (a) EL spectra recorded from the Au−Au junction as a function of bias voltage without laser illumination for increasing bias voltage (bottom to top). The blue curves represent Lorentzian line shapes fitted to the sub peaks. (b) Three types of spectral contributions represented by different peak positions form the bias voltage dependent luminescence spectra, reflecting three radiative LSP modes (1.39, 1.57, and 1.72 eV) that can be excited by IET in the junction. (c) Spectrally integrated luminescence intensities (solid squares) and the corresponding quantum efficiencies as a function of bias voltages.

and cryogenic temperatures.[39,40] Here, in Figure 2a we reproduce EL spectra from the Au−Au STM junction at ambient conditions without laser illumination. The numbers next to the spectra indicate the voltages at which the spectra were obtained. No photon emission is observed for bias voltages $|U_{bias}| \leq 1.25$ V. The first luminescence peak at about 890 nm starts to appear at $|U_{bias}| = 1.5$ V. For $|U_{bias}| \geq 2$ V, two further emission peaks at higher energy are observed. The spectral shape of the emission profile can be interpreted by the radiative decay of LSP modes in the tip−sample gap induced by IET and the observed LSP modes are in excellent qualitative agreement with results obtained at UHV conditions.[38,41] As shown in Figure 2a, the luminescence spectra are represented by fitting a model function (red line) composed of three Lorentzian curves (blue lines) which reflect the three LSP modes. Figure 2b plots the peak positions of the Lorentzian curves for all bias voltages and their mean values indicated by dashed lines, which reflect that the three LSP modes are located at about 1.39, 1.57, and 1.72 eV. Interestingly, although the peak positions of all three LSP modes stay almost constant, for positive bias voltages the mode at 1.57 eV has the highest intensity, whereas the mode at 1.72 eV shows the highest intensity for most negative

bias voltages. This could be a consequence of the asymmetric geometry of the Au−Au junction consisting of a sharp tip and a flat surface. Quantitatively, with the free electron model and the assumption of the tip radius a being much larger than the tip sample-distance d, the frequency of localized surface plasmon modes confined in a STM cavity can be expressed as[42]

$$\omega_n = \omega_p \left[\frac{\tanh\left(n+\frac{1}{2}\right)\beta_0}{\varepsilon^{(0)} + \tanh\left(n+\frac{1}{2}\right)\beta_0} \right]^{1/2}$$

$$\approx \sqrt{2}\omega_{sp} \left[\frac{\tanh(q_n d)}{\varepsilon^{(0)} + \tanh(q_n d)} \right]^{1/2} \quad (1)$$

where ω_p and ω_{sp} are the bulk and surface plasmon frequencies, respectively, $\beta_0 = \cosh^{-1}(1 + d/a)$, $q_n^{-1} = L_n = L/(2n + 1)$, $L = (2ad)^{1/2}$. L_n represents the lateral confinement length of the plasmon. According to eq 1 and taking ω_{sp} as 2.45 eV and d as 1.0 nm, we find that the three LSP modes obtained from the spectra correspond to the ω_2 (1.374 eV), ω_3 (1.569 eV), and ω_4 (1.720 eV) modes with the L being 26.5 nm.

Figure 2c shows the spectrally integrated luminescence intensity emitted from the Au−Au junction (without laser illumination) as a function of bias voltage. Although fluctuations are observed especially at higher bias voltages, the luminescence intensity has a general tendency to increase with increasing bias voltages. Assuming the density of states of the tip and sample vary only little in the relevant energy range, the photon emission intensity from the Au−Au junction due to IET (from energy level E to E $-$ $\hbar\omega$) can be described by the plasmon mode function $\Gamma(\hbar\omega)$ and the tunneling electron probability $T(E,U,z)$ as[39,40]

$$I_{IET}(\hbar\omega, eU) \propto \Gamma(\hbar\omega) \int_{\hbar\omega}^{eU} T(E, U, z)\, dE \quad (2)$$

where $T(E,U,z) \propto \exp\{-z[(4m/\hbar^2)(2\Phi + eU - 2E)]^{1/2}\}$, Φ is the barrier height above the sample Au (111), z is the tip−sample separation, and U is the applied bias voltage. Hence, the luminescence intensity increase can be estimated by the bias voltage dependent electron tunneling probability. The value of U only refers to the amplitude of the bias voltage, which means in the calculation that we assume symmetrical conditions for positive and negative bias voltages. With Φ = 5 eV and z = 1 nm, the calculated tunneling electron probability is plotted as a function of bias voltage (rescaled to the experimental data) as a solid line in Figure 2c, which shows a good agreement with the increasing tendency of the experimental results. The efficiency of photo emission due to IET can be estimated by the luminescence intensity and the tunneling current. Considering the constant tunneling current of 1 nA, the collected optical intensity of a few kilocounts per second (kcps) and the estimated

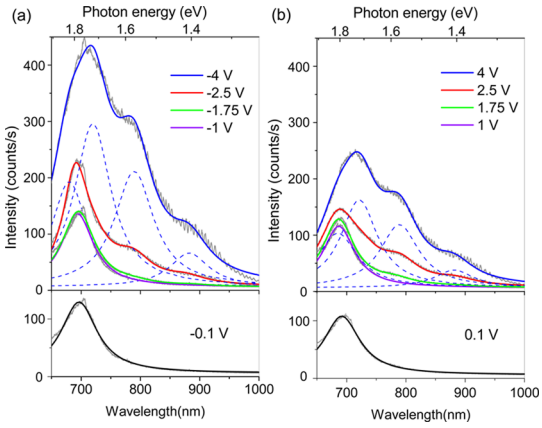

Figure 3. PL spectra (gray lines) and the fitting curves (solid smooth lines) of the laser illuminated Au−Au junction at negative (a) and positive (b) bias voltages. At low bias voltages ($|U_{bias}|$< 1.75 V), the spectral line shape consists of one band only and can be fitted by a single Lorentzian curve. As the bias voltage is increasing, further red-shifted bands appear. The dashed blue lines indicate the four Lorentzian fitting curves for the spectra obtained at −4 and 4 V, respectively.

photon collection efficiency of 1%, we calculate the quantum efficiency of about $\Gamma = 10^{-5}$ (photon per tunneling electron) of the pure IET luminescence. The study of photon emission from the Au−Au junction without laser illumination demonstrates the existence of three LSP modes generated by pure IET and their bias voltage dependence, providing information for elucidating the PL amplification from the same junction under laser illumination.

With the information on the IET induced LSP modes in the Au−Au junction, we further analyze the PL spectra of the junction under laser illumination. To quantitatively determine different contributions to the total PL intensity, we fit subpeaks to the spectral profiles for all bias voltages and show the results for the typical bias voltages in Figure (3). At the lowest bias voltages (±0.1 V), the recorded spectra can be fitted perfectly by one Lorentzian curve at about 690 nm, which indicates a single band emission. Furthermore, all PL spectra show the single band emission behavior for $|U_{bias}|$< 1.75 V. In these situations PL occurs due to electron−hole recombination and radiative inelastic plasmon relaxation.[7] The radiative plasmon emission has been observed also in gold nanoparticles under higher energy one photon excitation (*e.g.*, 3.3 eV).[43] The PL in the longer wavelength range (from 720 to 1050 nm) starts to be observed when $|U_{bias}|\geq$ 1.75 V. The dashed curves in Figure 3a,b represent the four Lorentzian peaks which are fitted to the spectra collected at the bias voltage of −4 V and +4 V, respectively. The peak positions of the fitted Lorentzian peaks of the PL at all bias voltages are plotted in Figure 4a. As a comparison, the radiative LSP modes of the junction obtained without laser illumination are plotted as solid dark green circles. As shown in Figure 4a, the three

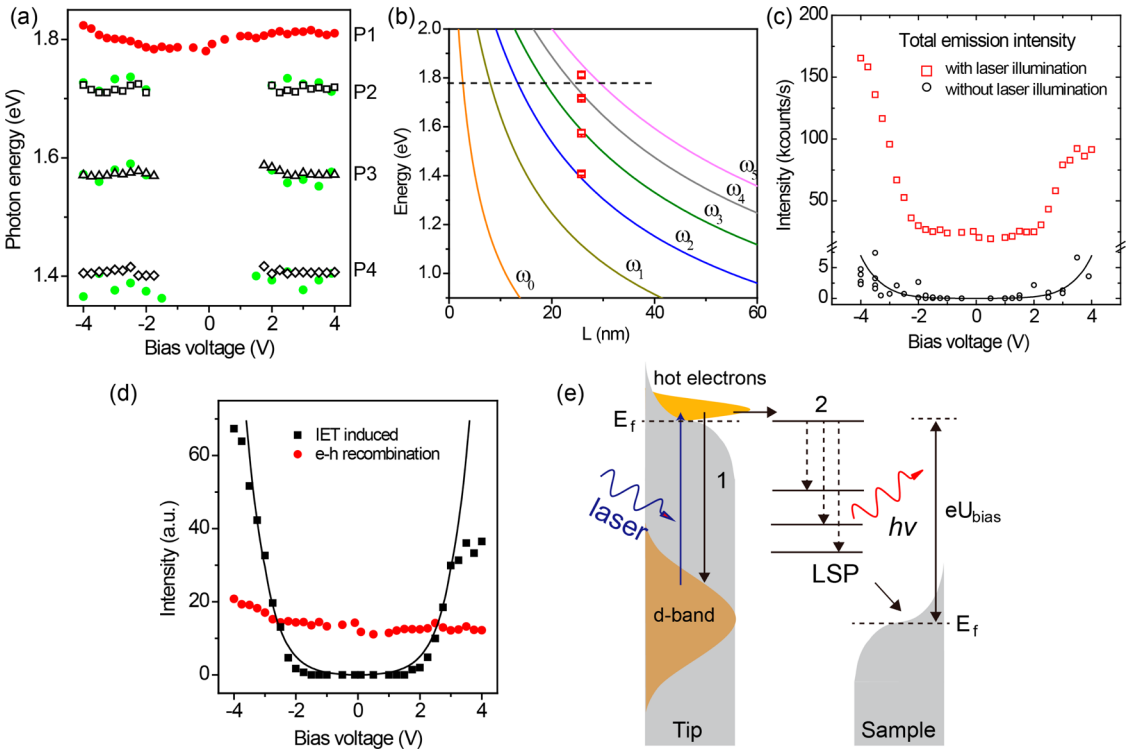

Figure 4. (a) Peak positions of PL bands due to laser excited electron−hole combination (P1) and IET (P2, P3, and P4). As a comparison, the three radiative LSP modes (solid green circles) excited by pure IET in the junction without laser illumination (as shown in Figure 2b) are plotted as well. (b) Experimentally obtained peak positions (red squares) and the calculated (based on eq 1) LSP modes frequencies ω_n as a function of lateral confinement length, L. The dashed line indicates the peak position of the purely optically excited plasmon (at −0.1 V). Hot electrons have a higher efficiency to excite gap modes than conduction electrons. (c) Comparison of the spectrally integrated total PL intensities as a function of bias voltage from the irradiated Au−Au junction (open red squares) and from the nonirradiated junction (open circles) (as in Figure 2c). (d) Intensity contributions from IET (solid squares) and electron−hole combination (solid circles) as a function of bias voltages under the laser illumination. (e) Sketch of the processes involved in an Au−Au junction under laser illumination as a function of bias voltage. Process (1) is related to electron−hole recombination and radiative inelastic plasmon relaxation. Process (2) is related to the radiative decay of local plasmon modes created by IET.

lower energy subpeaks (denoted by P2, P3, and P4) of the PL are located at about 1.72, 1.57, and 1.40 eV, which are fully consistent with those LSP modes induced by pure IET in the Au−Au junction without laser illumination. For the PL band with the high photon energy (denoted by P1) (red solid circles in Figure 4a), we observe a general blue-shift of the peak position from about 1.78 to 1.82 eV when the voltage increases from ±0.1 to ±4 V. In Figure 4b, the comparison of the experimentally observed peak positions and the LSP modes frequencies ω_n shows that the peak position of the PL band at the high photon energy (top square in Figure 4b) lies close to a higher (fifth) order LSP-mode of the junction.

Along with the appearance of the new PL bands, the total PL intensity increases dramatically when the bias voltage increases. The spectrally integrated PL intensity shown in Figure 4c under laser illumination reaches up to 100−160 kcps at higher bias voltages (±4 V), which is about five times higher than the intensity (20−25 kcps) recorded at lower bias voltages (±1 V). Furthermore, it is 2 orders of magnitude higher than the spectrally integrated purely IET induced luminescence. On the basis of the spectral fittings, different contributions to the total PL intensity can be distinguished. In Figure 4d, the spectrally integrated intensity of the PL band (P1) is plotted as red circles. The black squares represent the spectrally integrated intensity of the long wavelength bands (sum of P2, P,3 and P4), which appear when $|U_{bias}| \geq 1.75$ V. These are the photons created by IET. Hence, PL increase of the laser illuminated junction must be due to an amplification process which originates from laser-induced hot electrons close to the Fermi level.[44−46]

For our experimental configuration, illuminating the tip/sample junction with a focused laser beam polarized along the tip's axis, a coupled surface plasmon oscillation in the Au-tip and the underlying Au-surface is induced. It manifests itself as a highly localized surface charge oscillation at the very apex of the tip and the Au surface below. This oscillating surface charge constitutes an efficient source of hot electrons that can also contribute to IET or recombine with the holes in the d-band in addition to the conduction band electrons. Compared to the subfemtoseconds (fs) traveling time for electron tunneling,[47] the lifetime of hot electrons close to the Fermi levels is predicted to lie in the range of tens of femtoseconds

to picoseconds,[48] such that IET outperforms the nonradiative decay.

PL induced by inelastic tunneling increases rapidly and dominates the total PL at high bias voltages (solid squares in Figure 4d). The asymmetric increasing tendency of the luminescence intensity for bias voltages larger than 3 V could be due to the asymmetry of the geometric shape of the sharp Au tip and the planar Au surface across the junction, in which the hot electrons tunneling from the tip to the sample could be more efficient. The PL intensity referred to IET by hot electrons is proportional to the number of hot electrons and the tunneling probability. It can be described with a similar expression as eq 2:

$$I_{e-\mathrm{IET}}(\hbar\omega, eU) \propto \int_{\hbar\omega}^{e(U+U_0)} \rho(E)T(E, U, z)\, \mathrm{d}E \qquad (3)$$

where $\rho(E)$ is the hot electrons energy distribution, U_0 is the estimated energy difference of the hot electrons above the Fermi level. For fitting the experimental data in Figure 4d, we assume a single Gaussian distribution $\rho(E) = [1/\delta(2\pi)^{1/2}]e^{-\{[E-(U+U_0)]^2/2\delta^2\}}$ for the laser-induced hot electrons with center electron energy at $U_0 = 0.2$ eV higher than the Fermi level and a full width at half-maximum (fwhm) of 0.235 eV (for $\delta = 0.1$ eV). These values are chosen based on our experimental conditions such as excitation laser energy, electronic structures of Au and also due to their agreement with our experimental data. For bulk Au, the d-band electrons are about 1.86−2.2 eV (varies at different symmetry points) below the Fermi level.[49] Our diode laser photons have an energy of about 1.96 eV which is sufficient to excite electrons from the d-band to closely above the Fermi level. The excitation bandwidth needs to be considered as a convolution of the d-band electron distribution and the Fermi distribution. The fwhm of the measured PL spectrum of the bare tip and the tip−surface conjunction (in Figure 1d) is 0.25 and 0.20 eV, respectively, which is consistent with the results (fwhm in the range of 0.2−0.3 eV) reported by Raschke *et al.*[7] Since the PL spectrum reflects the plasmon mode of the system, the localized plasmon has the energy distribution (fwhm) in the range of 0.2−0.3 eV. Therefore, we estimate plasmon-induced hot electrons have a comparable energy distribution of 0.235 eV by taking δ as 0.1 eV.

The estimated bias voltage dependent PL due to the IET of hot electrons (the solid line in Figure 4d) shows a good agreement with the experimental results. Therefore, our experimental observations could be explained by a phenomenological model. Upon laser illumination, the total PL of the Au−Au junction can be divided into two processes, first purely laser-induced (electron−hole recombination) (fitting curve at the short wavelength: P1) and second IET involved (three fitting curves at the long wavelengths: P2, P3, and P4), which are drawn schematically as process 1 and 2 in Figure 4e, respectively. Hence, inelastic tunneling could offer an additional radiative decay channel for hot electrons in the tunneling junction. This can occur either *via* recombination of hot electrons with holes created in the d-band of the substrate and by direct radiative decay through the junctions' LSP-modes. At high bias voltage, the radiative tunneling of hot electrons from the tip outperforms recombination of hot electrons with holes in the d-band of the substrate. The plasmon line widths (Γ) obtained from the measured PL spectra of the pure tip (peak at 1.81 eV) and the tip−sample junction (at the bias of −0.1 V; emission peak at 1.78 eV) are 0.25 and 0.20 eV, corresponding to the plasmon lifetime ($\tau = 2\hbar/\Gamma$) of 5.3 and 6.6 fs, respectively. For the tip−sample junction formed at the low bias voltages, our findings are consistent with the results in ref 7. In these situation, the radiative Γ^{rad} and nonradiative Γ^{nrad} contributions are comparable. At high bias voltages, the electron tunneling process may open up new relaxation channels, which correspond to the three plasmon modes induced by inelastic electron tunneling. At −4 V, these three modes locate at 1.72, 1.57, and 1.40 eV with the spectral line widths of 0.18, 0.16, and 0.13 eV, respectively. Therefore, most likely due to the new relaxation channels, the summed total plasmon line width (Γ) is enlarged, which leads to a decreasing of the lifetime (τ).

CONCLUSIONS

In conclusion, we demonstrate how PL from an optically pumped Au−Au tunneling junction can be amplified by inelastic electron tunneling. On the basis of the fitting of the total photon emission profiles, we can distinguish the contributions of laser excited electron−hole recombination and electrons feeding into the gap modes by inelastic tunneling. We conclude that the increased photon emission mainly originates from radiative decay of the hot electrons closely above the Fermi-level *via* the inelastic tunneling plasmon modes. Our work extends the understanding and controlling of radiative relaxation in plasmonic systems. It would provide potential applications in plasmonic devices, such as an actively switchable nanoscale light source.

METHODS

All optical measurements were performed with a home-built parabolic mirror assisted tip enhanced near-field optical microscope based on tunneling current feedback. The tip scanning and current feedback are controlled by RHK SPM 100. The gold tips are produced by electrochemical etching of a 100 μm gold wire (ChemPur) with rectangular voltage pulses in concentrated hydrochloric acid (HCl). After etching, the tips are

rinsed thoroughly in distilled water to get rid of the retaining HCl. All tip were characterized by scanning electron microscopy. The gold substrate is a commercial gold (111) crystal with a diameter of 5 mm. Prior to the measurements, the crystal is cleaned by piranha solution (sulfuric acid, H_2SO_4, and hydrogen peroxide H_2O_2) and is further flame annealed for at least 5 min after rinsing with distilled water. For measurements with laser illumination, a diode laser (Picoquant LDH-D-C-640) is used as the excitation source. To illuminate the parabolic mirror completely, the diameter of the laser beam is expanded twice by telescopes. The linearly polarized Gaussian laser mode was converted to a radially polarized doughnut mode by four quarters half wave plates and a pinhole. A 50:50 beam splitter is used for reflecting excitation laser toward parabolic mirror and transmitting PL-signal from the junction to the detectors. One notch filter (6 optical density (OD)) and one long pass filter (6 OD) are used to eliminate the laser line from the detected signal. The signal is guided to a spectrometer (Acton Spectral Pro SP2300) combined with a charged coupled device (CCD) camera (Princeton Instruments Spec-10). The spectrometer is equipped with three gratings of 150, 600, and 1800 grooves/mm, providing different spectral resolutions. Auxiliary CCD cameras are used for monitoring the coarse positioning of the tip and the scattering pattern of the focus of the parabolic mirror. For measurements without laser illumination (light emission due to pure inelastic electron tunneling), after passing though the beam splitter, the signal is directly guided to the spectrometer without optical filters.

Conflict of Interest: The authors declare no competing financial interest.

Supporting Information Available: Laser power dependence of the PL of the bare gold tip. The Supporting Information is available free of charge on the ACS Publications website at DOI: 10.1021/acsnano.5b02361.

Acknowledgment. Financial support by the Projektförderung für Nachwuchswissenschaftler/Innen Uni-Tübingen and the DFG (Grant ME1600/5-3) is gratefully acknowledged.

REFERENCES AND NOTES

1. Schuller, J. A.; Barnard, E. S.; Cai, W.; Jun, Y. C.; White, J. S.; Brongersma, M. L. Plasmonics for Extreme Light Concentration and Manipulation. *Nat. Mater.* **2010**, *9*, 193–204.
2. Tame, M. S.; McEnery, K. R.; Ozdemir, S. K.; Lee, J.; Maier, S. A.; Kim, M. S. Quantum Plasmonics. *Nat. Phys.* **2013**, *9*, 329–340.
3. Halas, N. J.; Lal, S.; Chang, W.-S.; Link, S.; Nordlander, P. Plasmons in Strongly Coupled Metallic Nanostructures. *Chem. Rev.* **2011**, *111*, 3913–3961.
4. Huang, F.; Baumberg, J. J. Actively Tuned Plasmons on Elastomerically Driven Au Nanoparticle Dimers. *Nano Lett.* **2010**, *10*, 1787–1792.
5. Wustholz, K. L.; Henry, A.-I.; McMahon, J. M.; Freeman, R. G.; Valley, N.; Piotti, M. E.; Natan, M. J.; Schatz, G. C.; Duyne, R. P. V. Structure−Activity Relationships in Gold Nanoparticle Dimers and Trimers for Surface-Enhanced Raman Spectroscopy. *J. Am. Chem. Soc.* **2010**, *132*, 10903–10910.
6. Jain, P. K.; Huang, W.; El-Sayed, M. A. On the Universal Scaling Behavior of the Distance Decay of Plasmon Coupling in Metal Nanoparticle Pairs: A Plasmon Ruler Equation. *Nano Lett.* **2007**, *7*, 2080–2088.
7. Kravtsov, V.; Berweger, S.; Atkin, J. M.; Raschke, M. B. Control of Plasmon Emission and Dynamics at the Transition from Classical to Quantum Coupling. *Nano Lett.* **2014**, *14*, 5270–5275.
8. Anker, J. N.; Hall, W. P.; Lyandres, O.; Shah, N. C.; Zhao, J.; Van Duyne, R. P. Biosensing with Plasmonic Nanosensors. *Nat. Mater.* **2008**, *7*, 442–453.
9. Ghosh, S. K.; Pal, T. Interparticle Coupling Effect on the Surface Plasmon Resonance of Gold Nanoparticles: From Theory to Applications. *Chem. Rev.* **2007**, *107*, 4797–4862.
10. Hartschuh, A. Tip-Enhanced Near-Field Optical Microscopy. *Angew. Chem., Int. Ed.* **2008**, *47*, 8178–8191.
11. Pettinger, B.; Ren, B.; Picardi, G.; Schuster, R.; Ertl, G. Nanoscale Probing of Adsorbed Species by Tip-Enhanced Raman Spectroscopy. *Phys. Rev. Lett.* **2004**, *92*, 096101.
12. Anger, P.; Bharadwaj, P.; Novotny, L. Enhancement and Quenching of Single-Molecule Fluorescence. *Phys. Rev. Lett.* **2006**, *96*, 113002.
13. Zhang, D.; Heinemeyer, U.; Stanciu, C.; Sackrow, M.; Braun, K.; Hennemann, L. E.; Wang, X.; Scholz, R.; Schreiber, F.; Meixner, A. J. Nanoscale Spectroscopic Imaging of Organic Semiconductor Films by Plasmon-Polariton Coupling. *Phys. Rev. Lett.* **2010**, *104*, 056601.
14. Wang, X.; Zhang, D.; Braun, K.; Egelhaaf, H. J.; Brabec, C. J.; Meixner, A. J. High-Resolution Spectroscopic Mapping of the Chemical Contrast from Nanometer Domains in P3HT:PCBM Organic Blend Films for Solar-Cell Applications. *Adv. Funct. Mater.* **2010**, *20*, 492–499.
15. Wang, X.; Zhang, D.; Wang, Y. M.; Sevinc, P.; Luc, H. P.; Meixner, A. J. Interfacial Electron Transfer Energetics Studied by High Spatial Resolution Tip-Enhanced Raman Spectroscopic Imaging. *Angew. Chem., Int. Ed.* **2011**, *50*, A25–A29.
16. Neacsu, C. C.; Berweger, S.; Raschke, M. B. Tip-Enhanced Raman Imaging and Nanospectroscopy: Sensitivity, Symmetry, and Selection Rules. *NanoBiotechnology* **2007**, *3*, 172–196.
17. Berweger, S.; Neacsu, C. C.; Mao, Y. B.; Zhou, H. J.; Wong, S. S.; Raschke, M. B. Optical Nanocrystallography with Tip-Enhanced Phonon Raman Spectroscopy. *Nat. Nanotechnol.* **2009**, *4*, 496–499.
18. Hartschuh, A.; Sanchez, E. J.; Xie, X. S.; Novotny, L. High-Resolution Near-Field Raman Microscopy of Single-Walled Carbon Nanotubes. *Phys. Rev. Lett.* **2003**, *90*, 095503.
19. Yano, T.; Verma, P.; Saito, Y.; Ichimura, T.; Kawata, S. Pressure-Assisted Tip-Enhanced Raman Imaging at a Resolution of a Few Nanometres. *Nat. Photonics* **2009**, *3*, 473–477.
20. Steidtner, J.; Pettinger, B. Tip-enhanced Raman Spectroscopy and Microscopy on Single Dye Molecules with 15 nm Resolution. *Phys. Rev. Lett.* **2008**, *100*, 236101.
21. Zhang, R.; Zhang, Y.; Dong, Z. C.; Jiang, S.; Zhang, C.; Chen, L. G.; Zhang, L.; Liao, Y.; Aizpurua, J.; Luo, Y.; et al. Chemical Mapping of a Single Molecule by Plasmon-Enhanced Raman Scattering. *Nature* **2013**, *498*, 82–86.
22. Johansson, P.; Monreal, R.; Apell, P. Theory for Light Emission from a Scanning Tunneling Microscope. *Phys. Rev. B: Condens. Matter Mater. Phys.* **1990**, *42*, 9210–9213.
23. Berndt, R.; Gimzewski, J. K.; Johansson, P. Inelastic Tunneling Excitation of Tip-Induced Plasmon Modes on Noble-Metal Surfaces. *Phys. Rev. Lett.* **1991**, *67*, 3796–3799.
24. Persson, B. N. J.; Baratoff, A. Theory of Photon Emission in Electron Tunneling to Metallic Particles. *Phys. Rev. Lett.* **1992**, *68*, 3224–3227.
25. Nilius, N.; Ernst, N.; Freund, H. J. Photon Emission Spectroscopy of Individual Oxide-Supported Sliver Clusters in a Scanning Tunneling Microscope. *Phys. Rev. Lett.* **2000**, *84*, 3994–3997.
26. Dong, Z. C.; Zhang, X. L.; Gao, H. Y.; Luo, Y.; Zhang, C.; Chen, L. G.; Zhang, R.; Tao, X.; Zhang, Y.; Yang, J. L.; et al. Generation of Molecular Hot Electroluminescence by Resonant Nanocavity Plasmons. *Nat. Photonics* **2010**, *4*, 50–54.
27. Berndt, R.; Gaisch, R.; Gimzewski, J. K.; Reihl, B.; Schlittler, R. R.; Schneider, W. D.; Tschudy, M. Photon Emission at Molecular Resolution Induced by a Scanning Tunneling Microscope. *Science* **1993**, *262*, 1425–1427.
28. Qiu, X. H.; Nazin, G. V.; Ho, W. Vibrationally Resolved Fluorescence Excited with Submolecular Precision. *Science* **2003**, *299*, 542–546.
29. Savage, K. J.; Hawkeye, M. M.; Esteban, R.; Borisov, A. G.; Aizpurua, J.; Baumberg, J. J. Revealing the Quantum Regime in Tunnelling Plasmonics. *Nature* **2012**, *491*, 574–577.
30. Esteban, R.; Borisov, A. G.; Nordlander, P.; Aizpurua, J. Bridging Quantum and Classical Plasmonics with a Quantum-Corrected Model. *Nat. Commun.* **2012**, *3*, 825.

31. Fang, Y.; Chang, W.-S.; Willingham, B.; Swanglap, P.; Dominguez-Medina, S.; Link, S. Plasmon Emission Quantum Yield of Single Gold Nanorods as a Function of Aspect Ratio. *ACS Nano* **2012**, *6*, 7177–7184.
32. Wackenhut, F.; Failla, A. V.; Meixner, A. J. Multicolor Microscopy and Spectroscopy Reveals the Physics of the One-Photon Luminescence in Gold Nanorods. *J. Phys. Chem. C* **2013**, *117*, 17870–17877.
33. Lieb, M. A.; Meixner, A. J. A High Numerical Aperture Parabolic Mirror as Imaging Device for Confocal Microscopy. *Opt. Express* **2001**, *8*, 458–474.
34. Stadler, J.; Stanciu, C.; Stupperich, C.; Meixner, A. J. Tighter Focusing with a Parabolic Mirror. *Opt. Lett.* **2008**, *33*, 681–683.
35. Zuchner, T.; Failla, A. V.; Meixner, A. J. Light Microscopy with Doughnut Modes: A Concept to Detect, Characterize, and Manipulate Individual Nanoobjects. *Angew. Chem., Int. Ed.* **2011**, *50*, 5274–5293.
36. Pettinger, B.; Domke, K. F.; Zhang, D.; Schuster, R.; Ertl, G. Direct Monitoring of Plasmon Resonances in a Tip-Surface Gap of Varying Width. *Phys. Rev. B: Condens. Matter Mater. Phys.* **2007**, *76*, 113409.
37. Berndt, R.; Gimzewski, J. K.; Johansson, P. Electromagnetic-Interactions of Metallic Objects in Nanometer Proximity. *Phys. Rev. Lett.* **1993**, *71*, 3493–3496.
38. Meguro, K.; Sakamoto, K.; Arafune, R.; Satoh, M.; Ushioda, S. Origin of Multiple Peaks in the Light Emission Spectra of a Au(111) Surface Induced by the Scanning Tunneling Microscope. *Phys. Rev. B: Condens. Matter Mater. Phys.* **2002**, *65*, 165405.
39. Schneider, N. L.; Matino, F.; Schull, G.; Gabutti, S.; Mayor, M.; Berndt, R. Light Emission from a Double-Decker Molecule on a Metal Surface. *Phys. Rev. B: Condens. Matter Mater. Phys.* **2011**, *84*, 153403.
40. Reecht, G.; Scheurer, F.; Speisser, V.; Dappe, Y. J.; Mathevet, F.; Schull, G. Electroluminescence of a Polythiophene Molecular Wire Suspended between a Metallic Surface and the Tip of a Scanning Tunneling Microscope. *Phys. Rev. Lett.* **2014**, *112*, 047403.
41. Aizpurua, J.; Apell, S. P.; Berndt, R. Role of Tip Shape in Light Emission from the Scanning Tunneling Microscope. *Phys. Rev. B: Condens. Matter Mater. Phys.* **2000**, *62*, 2065–2073.
42. Rendell, R. W.; Scalapino, D. J. Surface Plasmons Confined by Microstructures on Tunnel Junctions. *Phys. Rev. B: Condens. Matter Mater. Phys.* **1981**, *24*, 3276–3294.
43. Dulkeith, E.; Niedereichholz, T.; Klar, T. A.; Feldmann, J.; von Plessen, G.; Gittins, D. I.; Mayya, K. S.; Caruso, F. Plasmon emission in photoexcited gold nanoparticles. *Phys. Rev. B: Condens. Matter Mater. Phys.* **2004**, *70*, 205424.
44. Knight, M. W.; Sobhani, H.; Nordlander, P.; Halas, N. J. Photodetection with Active Optical Antennas. *Science* **2011**, *332*, 702–704.
45. Mukherjee, S.; Libisch, F.; Large, N.; Neumann, O.; Brown, L. V.; Cheng, J.; Lassiter, J. B.; Carter, E. A.; Nordlander, P.; Halas, N. J. Hot Electrons Do the Impossible: Plasmon-Induced Dissociation of H2 on Au. *Nano Lett.* **2013**, *13*, 240–247.
46. Clavero, C. Plasmon-Induced Hot-Electron Generation at Nanoparticle/Metal-Oxide Interfaces for Photovoltaic and Photocatalytic Devices. *Nat. Photonics* **2014**, *8*, 95–103.
47. Wu, S. W.; Ogawa, N.; Ho, W. Atomic-Scale Coupling of Photons to Single-Molecule Junctions. *Science* **2006**, *312*, 1362–1365.
48. Manjavacas, A.; Liu, J. G.; Kulkarni, V.; Nordlander, P. Plasmon-Induced Hot Carriers in Metallic Nanoparticles. *ACS Nano* **2014**, *8*, 7630–7638.
49. Boyd, G. T.; Yu, Z. H.; Shen, Y. R. Photoinduced Luminescence from the Noble Metals and its Enhancement on Roughened Surfaces. *Phys. Rev. B: Condens. Matter Mater. Phys.* **1986**, *33*, 7923–7936.